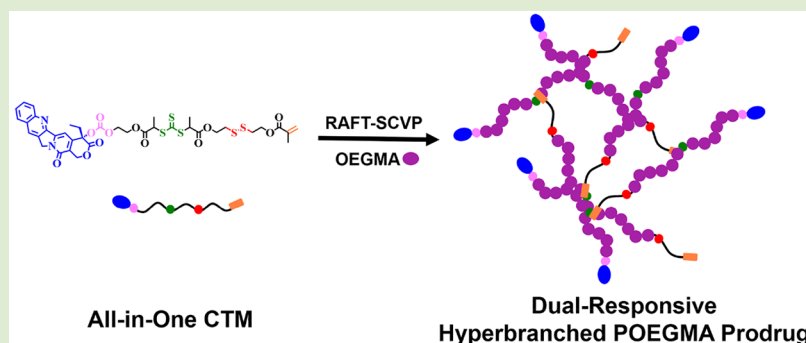


# One-Pot Synthesis of Dual-Responsive Hyperbranched Polymeric Prodrugs Using an All-in-One Chain Transfer Monomer

Yunfei Wang, Hua Wei,\*<sup>1</sup> Luping Zheng, Zhizhen Wu, Xiaolong Zhang, and Xianshuo Zhang

State Key Laboratory of Applied Organic Chemistry, Key Laboratory of Nonferrous Metal Chemistry and Resources Utilization of Gansu Province, and College of Chemistry and Chemical Engineering, Lanzhou University, Lanzhou, Gansu 730000, China

## Supporting Information



**ABSTRACT:** Over the past decades, tremendous progress has been advanced in the preparation of hyperbranched polymers (HPs), especially for the one-pot synthesis of segmented HPs by using self-condensing vinyl polymerization based on controlled living radical polymerization techniques. However, the fabrication of hyperbranched polymeric prodrugs (HPPs) still requires multistep postpolymerization conjugations, which generally suffer from low and uncontrolled conjugation efficacy of drug molecules due to the steric hindrance, low yields because of multistep synthesis, and scale-up difficulties attributed to batch-to-batch variations. To further address these issues and provide a highly straightforward and robust strategy toward HPPs, we reported in this study the one-pot preparation of dual-responsive hyperbranched polymeric prodrugs (DRHPPs) using an all-in-one chain transfer monomer that integrates a drug molecule with both acidic pH- and reduction-sensitive links. The resulting DRHPPs with precisely regulated drug loading content and great therapeutic efficacy offered a highly promising platform for efficient anticancer drug delivery.

Hyperbranched polymers (HPs),<sup>1–3</sup> compared to the traditional linear polymers with an identical molecular weight (MW), possess various advantages, such as a three-dimensional (3D) highly branched globular structure, smaller hydrodynamic radius, lower solution or melt viscosity, multivalent surface with more functionalities, no or lower chain entanglement, greater solubility, and capacity to form unimolecular micelles with enhanced stability;<sup>4,5</sup> thus, they have attracted considerable attention as carriers for drug delivery.<sup>6–8</sup> Although tremendous progress has been advanced in the preparation of HPs, especially for the one-pot synthesis of segmented hyperbranched polymers (SHPs) by using self-condensing vinyl polymerization (SCVP) based on controlled living radical polymerization (CLRPP) techniques such as reversible addition–fragmentation chain transfer (RAFT) polymerization and atom transfer radical polymerization (ATRP),<sup>9–12</sup> the fabrication of hyperbranched polymeric prodrugs (HPPs) still requires multistep postpolymerization conjugations, which generally suffer from low and uncontrolled conjugation efficacy of drug molecules due to the steric hindrance of SHPs, low yields because of multistep synthesis,

and scale-up difficulties attributed to batch-to-batch variations.<sup>13–16</sup>

One notable strategy recently developed to address the drawbacks mentioned above is adoption of a drug-based monomer.<sup>17,18</sup> To provide a highly straightforward and robust alternative toward HPPs, herein we designed and synthesized an all-in-one chain transfer monomer (ACTM), integrating a drug molecule with both acidic pH- and reduction-sensitive links (Scheme 1).

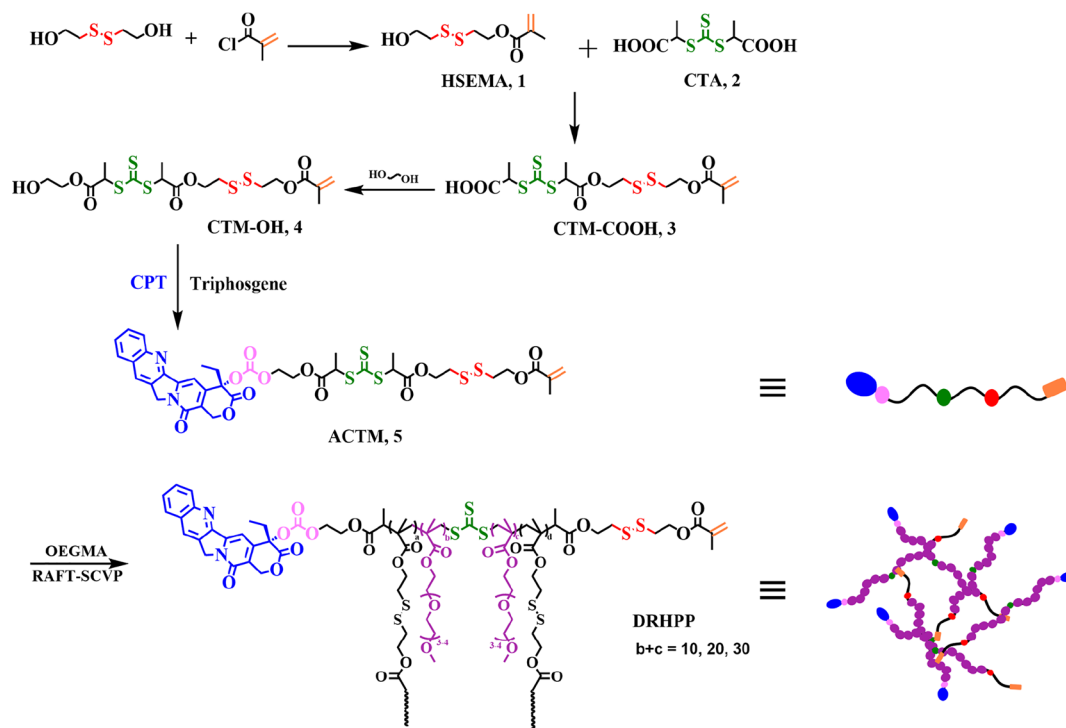
To demonstrate the utility of this ACTM, a one-pot synthesis of well-defined, dual-responsive hyperbranched polymeric prodrugs (DRHPPs) was further performed using ACTM-mediated RAFT-SCVP of oligo(ethylene glycol methyl ether methacrylate) (OEGMA; Scheme 1). The therapeutic efficacy of the resulting DRHPPs was evaluated by in vitro drug release, cellular uptake, and cytotoxicity studies.

First, ACTM was synthesized by four consecutive esterification reactions, including (i) synthesis of HSEMA

Received: August 10, 2018

Accepted: September 13, 2018

## Scheme 1. Synthetic Route of ACTM and DRHPPs



(1), (ii) DCC coupling between HSEMA (1) and CTA (2) to generate reducible CTM with carboxylic terminus (CTM-COOH, 3), (iii) terminal conversion of CTM-COOH from carboxyl to hydroxyl to produce CTM-OH (4), and (iv) synthesis of target ACTM by conjugating camptothecin (CPT) to CTM-OH via a carbonate link in the presence of triphosgene. The successful synthesis of ACTM was confirmed by <sup>1</sup>H NMR (Figure 1), <sup>13</sup>C NMR (Figure S5a), and high

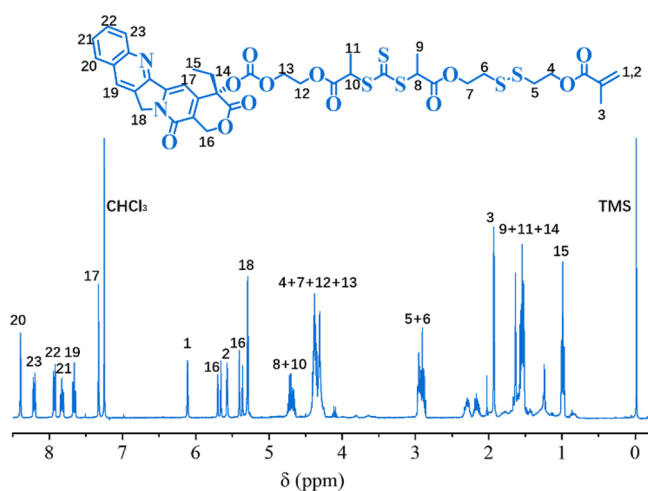
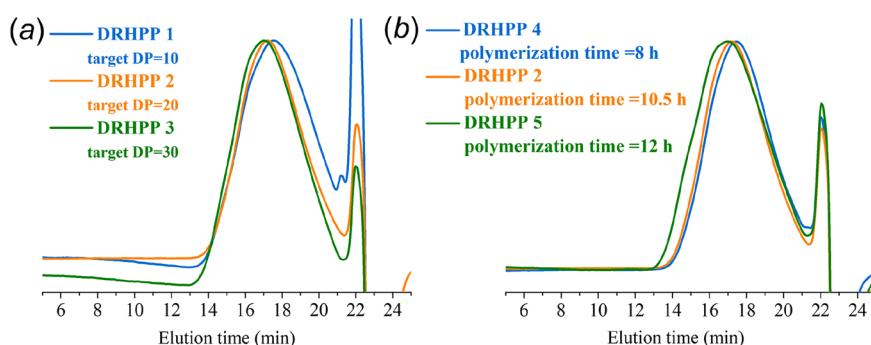


Figure 1. <sup>1</sup>H NMR spectrum of ACTM in CDCl<sub>3</sub>.

resolution mass spectral (HRMS; Figure S5b, *m/z* = 877) analyses. The synthesized ACTM integrates triple functions of a CTM structure for generation of HPs, a CPT molecule for simultaneous production of prodrugs, and dual-responsive (acidic pH-sensitive carbonate group and reduction-responsive disulfide bridge) links for efficient intracellular polymer degradation and drug release.

Next, we prepared DRHPPs by ACTM-mediated RAFT-SCVP of OEGMA under various polymerization conditions. Three different target degrees of polymerization (DPs) of 10, 20, and 30 were adopted to prepare DRHPP1, 2, and 3, respectively. Further screening by the symmetry and polydispersity (*D*) of the size exclusion chromatography (SEC) elution peaks of the synthesized polymers reveals a slightly better target DP of 20 relative to those of 10 and 30 for the polymer preparation (Figure 2a). Polymerizations were thus conducted at various polymerization time points using this optimal target DP of 20. A distinguishable shift toward higher molecular weight (MW) was recorded with increasing polymerization time for DRHPP4, 2, and 5, which confirms the successful synthesis of DRHPPs in a controlled manner (Figure 2b). Note that DRHPPs, prepared with the longest polymerization time, showed the appearance of a slight shoulder in the high-MW side of its SEC elution peak, which is most likely relevant to the coupling reactions between chain radicals in RAFT-SCVP.<sup>10</sup> Typically, the actual DP of the DRHPP2 was determined to be 21 by comparing the ratio of the integrated intensity of the peak at 5.30 ppm attributed to the methylene protons adjacent to the CPT to that of the peak at 3.37 ppm assigned to the methoxyl protons adjacent to OEGMA in the <sup>1</sup>H NMR spectrum (Figure S6). The MW, *D*, each branched repeat unit (RB), and number-average CTA functionality per branched copolymer (*F*) of all the synthesized DRHPPs are summarized in Table 1.

The critical micelle concentration (CMC) and average size of micelles self-assembled by DRHPPs were then studied. The CMCs were determined using pyrene as a fluorescence probe,<sup>19</sup> and all the four DRHPPs showed similar and extremely low CMC values of approximately 3.0 mg/L (Figure S7), likely implying their capability to form unimolecular micelles with enhanced stability. The average sizes of self-assembled micelles were measured by DLS at a concentration



**Figure 2.** SEC elution traces of (a) DRHPP1–3 with target degrees of polymerization of 10, 20, and 30 and (b) DRHPP2, 4, 5 with polymerization times of 8, 10.5, and 12 h using DMF as the eluent.

**Table 1. Summary of RAFT-SCVP Polymerization of ACTM with OEGMA under Various Conditions**

|        | target DP <sup>a</sup> | time <sup>a</sup> (h) | M <sub>n</sub> <sup>b</sup> (kDa) | D <sup>b</sup> | RB <sup>c</sup> | F     |
|--------|------------------------|-----------------------|-----------------------------------|----------------|-----------------|-------|
| DRHPP1 | 10                     | 10.5                  | 109.7                             | 2.1            | 10.0            | 36.0  |
| DRHPP2 | 20                     | 10.5                  | 64.8                              | 2.3            | 21.1            | 10.24 |
| DRHPP3 | 30                     | 10.5                  | 102.1                             | 2.6            | 28.4            | 12.2  |
| DRHPP4 | 20                     | 8                     | 76.1                              | 2.2            | 21.2            | 11.9  |
| DRHPP5 | 20                     | 12                    | 93.3                              | 2.9            | 21.2            | 14.7  |

<sup>a</sup>Polymerization conditions: [OEGMA] = 0.6 mol/L in DMAc at 70 °C. <sup>b</sup>Determined by SEC-MALLS. <sup>c</sup>Determined by <sup>1</sup>H NMR analysis.

of 0.5 mg/mL, well above their CMCs in both water and PBS, to evaluate the micelle stability in water and physiological salt condition (Figure S8). Notably, the DRHPP5 micelles showed dual-modal populations with the broadest size distribution in PBS (pH 7.4), which agrees well with the largest  $D$  of the polymer (Table 1). In contrast, the DRHPP2 micelles showed

quite similar mean sizes, with both unimodal narrow size distributions in water and PBS (66.7 nm, 0.219 vs 74.5 nm, 0.239), strongly supporting their best salt stability in contrast to the instability of the other three micelle constructs. The ability of DRHPP2 to form unimolecular micelles was further evaluated using *N,N'*-dimethylformamide (DMF) that is a good solvent for all the moieties of DRHPP2 as the medium. Given the nonoccurrence of self-assembly of DRHPP2 into micelles in DMF, the polymer size determined by DLS in DMF at a polymer concentration of 1 mg/mL revealed a mean diameter of 25.5 nm for unimolecular micelles of DRHPP2, which is slightly larger than those determined in H<sub>2</sub>O (14.6 nm) and PBS (pH 7.4, 15.2 nm) at a diluted concentration of 0.125 mg/mL (Figure S9). The results confirm somewhat swelling of DRHPP2 in DMF relative to aqueous media as well as formation of unimolecular micelles by DRHPP2. TEM observation further revealed formation of well-dispersed spherical DRHPP2 micelles with almost identical average

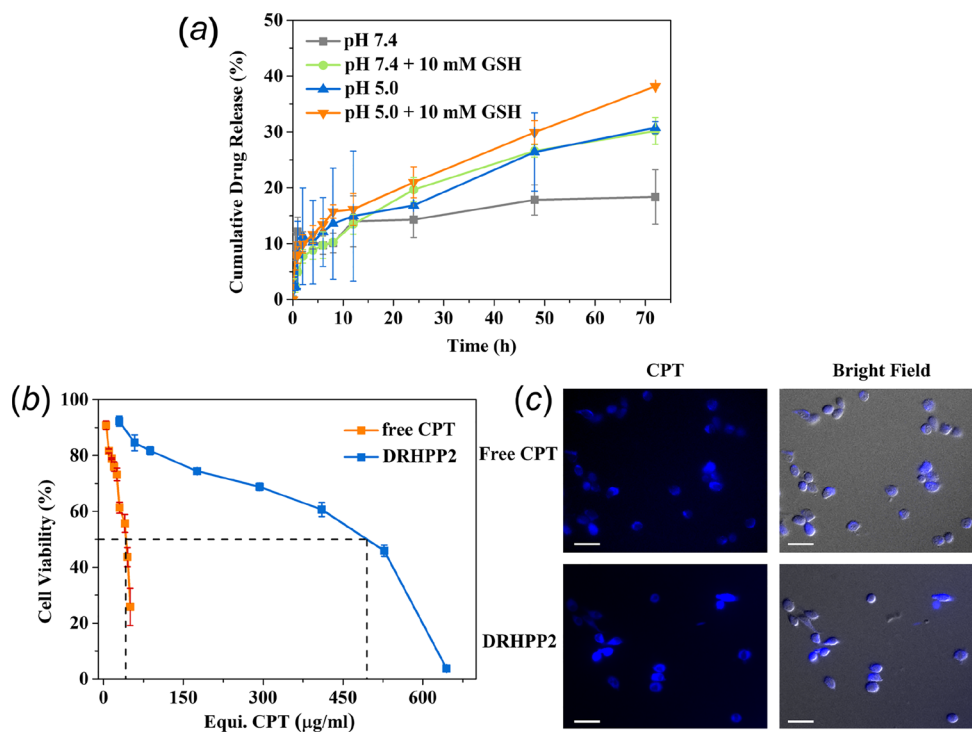


**Figure 3.** (a) In vitro drug release profiles of DRHPP2 prodrugs under various conditions. (b) In vitro cytotoxicity of free CPT and DRHPP2 prodrugs in HeLa cells. Cell viability was determined by MTS assay and expressed as % viability compared to untreated cells control. (c) Fluorescence images of HeLa cells incubated with free CPT and DRHPP2 for 4 h. The scale bar represents 20 μm.

sizes of approximately 10.7 and 13.7 nm in H<sub>2</sub>O and DMF at a concentration of 0.125 and 1 mg/mL (Figure S10), respectively. Therefore, the results are in good agreement with the DLS data, supporting unimolecular micelle formation for DRHPP2. Such a small size of the unimolecular DRHPP2 micelles together with their enhanced stability can promote passive targeting via the so-called enhanced permeation and retention (EPR) effect, as well as minimize the clearance by the reticuloendothelial system (RES) in the liver.<sup>20</sup> The long-term stability of unimolecular DRHPP2 micelles was further evaluated by monitoring the size change of the micelle solution incubated in PBS (pH 7.4) at 37 °C for different periods of 1, 7, and 20 days, which showed a constant size at around 16 nm, with negligible variation during the examined duration (Figure S11), as does the size distribution (data not shown). The results confirm the apparent stability of unimolecular DRHPP2 micelles, which is highly desirable for *in vivo* applications. Therefore, DRHPP2 micelle construct was chosen for further characterizations and biological evaluations.

The reduction and acidic pH-triggered degradation of DRHPP2 micelles was investigated by monitoring the size change under various conditions by DLS (Figure S12). As expected, the exertion of either single stimulus (pH 5.0 or 10 mM GSH) or both triggers promoted the destabilization of DRHPP2 micelles, as evidenced by the dramatic alteration of size at different time points, in contrast to the consistently unaltered size recorded at pH 7.4. Such change of size seems a complex process, which is most likely relevant to the reduction-triggered cleavage of disulfide bridge, acidic pH-induced hydrolysis of carbonate link in the polymer structure, and subsequent release of free CPT molecules, as well as degradation of the HP structure into linear POEGMA chains. The products incubated at pH 5.0 with 10 mM GSH for different periods of 6, 12, and 24 h were further subjected to size exclusion chromatography and multiangle laser light scattering (SEC-MALLS) analyses (Figure S13), which clearly reveals a time-dependent shift of the SEC elution peaks of the degraded products toward lower MW (longer retention time). The results support the dual stimuli-triggered degradation of DRHPP2 into low MW species.

Next, the *in vitro* drug loading and drug release profiles of DRHPP2 micelles were investigated. It is important to note that the actual drug loading content (DLC) of DRHPP2 formulation was determined to be 5.86% by measuring the UV–vis absorbance of CPT at 369 nm. Such a value is in close agreement with the calculated theoretical DLC of DRHPP2 (5.69%), demonstrating the precisely controlled DLC using the all-in-one CTM-mediated RAFT-SCVP.

*In vitro* drug release profiles of DRHPP2 micelles were then investigated under various conditions (Figure 3a), adopted for a DLS-monitored degradation study. Notably, the cumulative drug release under exertion of single stimulus (pH 5.0 or 10 mM GSH) reached 30% relative to 18% obtained at pH 7.4 in 72 h and further increased to nearly 40% under both triggers, which indicates the significant promotion of drug release by simultaneous application of both acidic pH and reduction stimuli relative to those acquired under single trigger.

Finally, the *in vitro* cytotoxicity and cellular uptake of DRHPP2 micelles in HeLa cells were assessed by 3-(4,5-dimethylthiazol-2-yl)-5-(3-carboxymethoxyphenyl)-2-(4-sulphophenyl)-2H-tetrazolium (MTS) cell viability assay and fluorescence microscope, respectively, to evaluate the delivery efficacy of DRHPP2 formulation. The half maximal inhibitory

concentrations (IC<sub>50</sub>) of free CPT and DRHPP2 were determined to be 39.1 ± 0.7 and 380.3 ± 3.89 μg mL<sup>-1</sup>, respectively (Figure 3b). The DRHPP2 micelles exhibited less cytotoxic activity than the free CPT likely due to their different internalization mechanisms (endocytosis vs direct membrane permeation) and the release kinetics of free drug from the polymeric prodrugs. It is important to note that the antiproliferation effect of DRHPP2 observed in HeLa cells is contributed simultaneously by the released active CPT after intracellular uptake of the polymer construct and CPT that is released by the cleavage of the carbonate link in the extracellular tumor environment with a weakly acidic pH of 6.8, both of which might be useful still for drug delivery. In the fluorescence images (Figure 3c), the strongly blue fluorescence of CPT could be readily observed in HeLa cells for both incubation with free CPT and CPT in DRHPP2 micelles for 4 h, suggesting that the drug was transported successfully by the micelle prodrug to the cells and, subsequently, underwent intracellular trafficking in a pattern consistent with the free drug.

In summary, we synthesized an ACTM as a highly straightforward and robust strategy toward one-pot fabrication of DRHPP. The resulting DRHPP with enhanced stability, precisely controlled DLC, and dual stimuli-triggered polymer degradation and drug release, as well as efficient cellular uptake further provided a highly promising platform toward efficient anticancer drug delivery.

## ■ ASSOCIATED CONTENT

### 📄 Supporting Information

The Supporting Information is available free of charge on the ACS Publications website at DOI: 10.1021/acsmacrolett.8b00603.

Experimental details and additional characterizations including <sup>1</sup>H NMR spectra of HSEMA and CTA, <sup>1</sup>H, <sup>13</sup>C NMR, HRMS data of CTM-COOH and CTM-OH, <sup>13</sup>C NMR, HRMS data of ACTM, <sup>1</sup>H NMR spectrum of DRHPP2, CMC determinations of DRHPPs, DLS data of DRHPPs in various solvents, TEM images of DRHPP2, salt stability evaluation of DRHPP2 by DLS, size variations and degradation behaviors of DRHPP2 monitored by DLS and SEC-MALLS are available in Figures S1–S13 (PDF).

## ■ AUTHOR INFORMATION

### Corresponding Author

\*E-mail: weih@lzu.edu.cn.

### ORCID

Hua Wei: 0000-0002-5139-9387

### Notes

The authors declare no competing financial interest.

## ■ ACKNOWLEDGMENTS

The authors acknowledge the financial support from the National Natural Science Foundation of China (51473072 and 21504035), the Thousand Young Talent Program, and the Open Research Fund of State Key Laboratory of Polymer Physics and Chemistry, Changchun Institute of Applied Chemistry, Chinese Academy of Sciences.

## REFERENCES

- (1) Wang, D.; Zhao, T.; Zhu, X.; Yan, D.; Wang, W. Bioapplications of Hyperbranched Polymers. *Chem. Soc. Rev.* **2015**, *44*, 4023–4071.
- (2) Zheng, Y.; Li, S.; Weng, Z.; Gao, C. Hyperbranched Polymers: Advances from Synthesis to Applications. *Chem. Soc. Rev.* **2015**, *44*, 4091–4130.
- (3) Jiang, W.; Zhou, Y.; Yan, D. Hyperbranched Polymer Vesicles: from Self-Assembly, Characterization, Mechanisms, and Properties to Applications. *Chem. Soc. Rev.* **2015**, *44*, 3874–3889.
- (4) Tomalia, D. A.; Fréchet, J. M. J. Discovery of Dendrimers and Dendritic Polymers: A Brief Historical Perspective. *J. Polym. Sci., Part A: Polym. Chem.* **2002**, *40*, 2719–2728.
- (5) Voit, B. I.; Lederer, A. Hyperbranched and Highly Branched Polymer Architectures—Synthetic Strategies and Major Characterization Aspects. *Chem. Rev.* **2009**, *109*, 5924–5973.
- (6) Rezaei, S. J. T.; Abandansari, H. S.; Nabid, M. R.; Niknejad, H. pH-Responsive Unimolecular Micelles Self-assembled from Amphiphilic Hyperbranched Block Copolymer for Efficient Intracellular Release of Poorly Water-Soluble Anticancer Drugs. *J. Colloid Interface Sci.* **2014**, *425*, 27–35.
- (7) Prabakaran, M.; Grailer, J. J.; Pilla, S.; Steeber, D. A.; Gong, S. Folate-Conjugated Amphiphilic Hyperbranched Block Copolymers Based on Boltorn H40, Poly(*l*-lactide) and Poly(ethylene glycol) for Tumor-Targeted Drug Delivery. *Biomaterials* **2009**, *30*, 3009–3019.
- (8) Liu, J.; Pang, Y.; Huang, W.; Huang, X.; Meng, L.; Zhu, X.; Zhou, Y.; Yan, D. Bioreducible Micelles Self-Assembled from Amphiphilic Hyperbranched Multiarm Copolymer for Glutathione-Mediated Intracellular Drug Delivery. *Biomacromolecules* **2011**, *12*, 1567–1577.
- (9) Zhang, M.; Liu, H.; Shao, W.; Ye, C.; Zhao, Y. Versatile Synthesis of Multiarm and Mikroarm Star Polymers with a Branched Core by Combination of Menschutkin Reaction and Controlled Polymerization. *Macromolecules* **2012**, *45*, 9312–9325.
- (10) Zhang, C.; Zhou, Y.; Liu, Q.; Li, S.; Perrier, S.; Zhao, Y. Facile Synthesis of Hyperbranched and Star-Shaped Polymers by RAFT Polymerization Based on a Polymerizable Trithiocarbonate. *Macromolecules* **2011**, *44*, 2034–2049.
- (11) Muthukrishnan, S.; Mori, H.; Müller, A. H. E. Synthesis and Characterization of Methacrylate-Type Hyperbranched Glycopolymers via Self-Condensing Atom Transfer Radical Copolymerization. *Macromolecules* **2005**, *38*, 3108–3119.
- (12) Min, K.; Gao, H. New Method to Access Hyperbranched Polymers with Uniform Structure via One-Pot Polymerization of Inimer in Microemulsion. *J. Am. Chem. Soc.* **2012**, *134*, 15680–15683.
- (13) Zhou, X.; Chang, C.; Zhou, Y.; Sun, L.; Xiang, H.; Zhao, S.; Ma, L.; Zheng, G.; Liu, M.; Wei, H. A Comparison Study to Investigate the Effect of Drug-Loading Site on Its Delivery Efficacy Using Double Hydrophilic Block Copolymers-Based Prodrugs. *J. Mater. Chem. B* **2017**, *5*, 4443–4454.
- (14) Yang, X.; Grailer, J. J.; Pilla, S.; Steeber, D. A.; Gong, S. Tumor-Targeting, pH-Responsive, and Stable Unimolecular Micelles as Drug Nanocarriers for Targeted Cancer Therapy. *Bioconjugate Chem.* **2010**, *21*, 496–504.
- (15) Wang, C. E.; Wei, H.; Tan, N.; Boydston, A. J.; Pun, S. H. Sunflower Polymers for Folate-Mediated Drug Delivery. *Biomacromolecules* **2016**, *17*, 69–75.
- (16) Zheng, L.; Wang, Y.; Zhang, X.; Ma, L.; Wang, B.; Ji, X.; Wei, H. Fabrication of Hyperbranched Block-Statistical Copolymer-Based Prodrug with Dual Sensitivities for Controlled Release. *Bioconjugate Chem.* **2018**, *29*, 190–202.
- (17) Hu, X.; Hu, J.; Tian, J.; Ge, Z.; Zhang, G.; Luo, K.; Liu, S. Polyprodrug Amphiphiles: Hierarchical Assemblies for Shape-Regulated Cellular Internalization, Trafficking, and Drug Delivery. *J. Am. Chem. Soc.* **2013**, *135*, 17617–17629.
- (18) Zhang, W.-J.; Hong, C.-Y.; Pan, C.-Y. Fabrication of Reductive-Responsive Prodrug Nanoparticles with Superior Structural Stability by Polymerization-Induced Self-Assembly and Functional Nanoscopic Platform for Drug Delivery. *Biomacromolecules* **2016**, *17*, 2992–2999.
- (19) Zhang, X.; Zhang, M.; Wang, M.; Peng, H.; Hua, Q.; Ma, L.; Wang, B.; Wei, H. Facile Fabrication of 10-Hydroxycamptothecin-Backboned Amphiphilic Polyprodrug with Precisely Tailored Drug Loading Content for Controlled Release. *Bioconjugate Chem.* **2018**, *29*, 2239–2247.
- (20) Wang, C. E.; Stayton, P. S.; Pun, S. H.; Convertine, A. J. Polymer Nanostructures Synthesized by Controlled Living Polymerization for Tumor-Targeted Drug Delivery. *J. Controlled Release* **2015**, *219*, 345–354.